Infection-Induced Regulation of Natural Killer Cells by Macrophages and Collagen at the Lymph Node Subcapsular Sinus

Janine L. Coombes,[1,2] Seong-Ji Han,[1] Nico van Rooijen,[3] David H. Raulet,[1] and Ellen A. Robey[1,*]
[1]Department of Molecular and Cell Biology, Life Sciences Addition, University of California, Berkeley, Berkeley, CA 94720, USA
[2]Sir William Dunn School of Pathology, University of Oxford, South Parks Road, Oxford OX1 3RE, UK
[3]Department of Molecular Cell Biology, Vrije Universiteit, Vrije Universiteit Medical Center, Amsterdam 1081 BT, The Netherlands
*Correspondence: erobey@berkeley.edu
http://dx.doi.org/10.1016/j.celrep.2012.06.001

SUMMARY

Infection leads to heightened activation of natural killer (NK) cells, a process that likely involves direct cell-to-cell contact, but how this occurs in vivo is poorly understood. We have used two-photon laser-scanning microscopy in conjunction with *Toxoplasma gondii* mouse infection models to address this question. We found that after infection, NK cells accumulated in the subcapsular region of the lymph node, where they formed low-motility contacts with collagen fibers and CD169^{+} macrophages. We provide evidence that interactions with collagen regulate NK cell migration, whereas CD169^{+} macrophages increase the activation state of NK cells. Interestingly, a subset of CD169^{+} macrophages that coexpress the inflammatory monocyte marker Ly6C had the most potent ability to activate NK cells. Our data reveal pathways through which NK cell migration and function are regulated after infection and identify an important accessory cell population for activation of NK cell responses in lymph nodes.

INTRODUCTION

Lymph nodes and other organized lymphoid tissues help to orchestrate interactions between immune cells and pathogens during infection, thus dictating the nature of immune responses and the outcome of infection. Recent advances in fluorescent labeling of living immune cells and pathogens, and imaging methods to detect these labels within tissues, now make it possible to probe events during in vivo infection with high spatial and temporal resolution. As a result, our understanding of the nature of interactions between immune cells and pathogens during infection is advancing at a rapid pace (Coombes and Robey, 2010).

Cellular interactions are particularly important for natural killer (NK) cells, which despite their name, often require priming by an accessory cell population for optimal effector function. The best described of these interactions occurs between dendritic cells (DCs) and NK cells, but macrophages and monocytes are also capable of potentiating NK cell effector function (Fernandez et al., 1999; Lucas et al., 2007; Newman and Riley, 2007; Dalbeth et al., 2004; Baratin et al., 2005; Soderquest et al., 2011). Activation of NK cells can be mediated by cell surface molecules such as NKG2D ligands and by cytokines including IL-12, IL-18, IL-15, and type I IFN. In vitro assays revealed the formation of stable contacts between DCs and NK cells (Borg et al., 2004; Brilot et al., 2007). Moreover, activation of NK cells by accessory cells generally requires close proximity between the cell types, even when activation is mediated by cytokines. For example synaptic delivery of IL-12 is necessary for IFN-γ secretion by NK cells, whereas IL-15 must be transpresented by IL-15Rα expressing accessory cells to activate NK cells (Borg et al., 2004; Koka et al., 2004; Lucas et al., 2007; Mortier et al., 2008).

Lymph nodes provide a potential site for interaction between NK cells and accessory cells under inflammatory conditions. Colocalization of NK cells with DCs has been demonstrated in human and murine lymph node sections, and NK cells are recruited to lymph nodes following injection of mature DCs (Bajénoff et al., 2006; Ferlazzo et al., 2004; Martín-Fontecha et al., 2004; Walzer et al., 2007). Study of NK cell motility in lymph nodes following poly I:C treatment revealed that NK cells formed multiple, short-lived interactions with DCs (Beuneu et al., 2009). Although short lived, these interactions appear to be crucial because NK activation did not occur in dissociated tissue but required the presence of an intact lymph node (Beuneu et al., 2009). In contrast, NK cells engaged in long-lived contacts with DCs in both uninflamed and *Leishmania major*-infected lymph nodes (Bajénoff et al., 2006).

In addition to interactions with accessory cells, interactions with the extracellular matrix may also regulate NK cell function. NK cells express high levels of CD49b, an integrin subunit that forms a receptor for collagen. Despite being used for many years to identify NK cells, surprisingly little is known about its functional role (Arase et al., 2001). A recent study demonstrated that CD49b crosslinking increased adherence of NK cells to collagen fibers, inhibited cytotoxicity, and promoted IFN-γ production (Garrod et al., 2007). However, whether this interaction regulates NK cell motility and function in vivo during infection has not been explored. In fact whereas a variety of signals are capable of regulating NK cells, the cell-cell interactions and spatial cues that influence NK cell function during in vivo infection remain unclear.
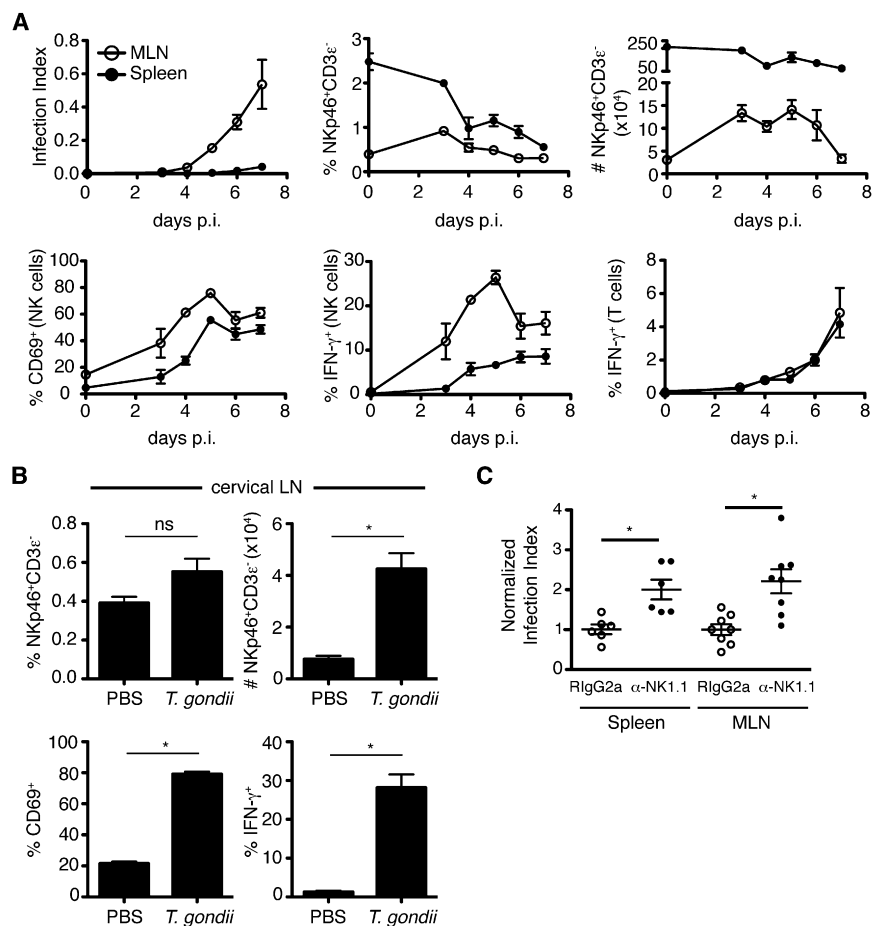
Figure 1. NK Cells Are Activated following Oral *T. gondii* Infection and Limit Parasite Burden

(A) Flow cytometric analysis of spleen (closed symbols) and mesenteric lymph node (open symbols) at days 3–7 following oral infection is presented. Graphs show Infection Index (percentage of cells in the live gate containing fluorescent parasites), percentage of NKp46$^+$ CD3ε$^-$ NK cells among live cells, total number of NKp46$^+$CD3ε$^-$ NK cells, percentage of CD69$^+$ cells among NKp46$^+$CD3ε$^-$ NK cells, percentage of IFN-γ$^+$ cells among NKp46$^+$CD3ε$^-$ NK cells, and percentage of IFN-γ$^+$ cells among CD3ε$^+$ T cells (mean ± SEM of three mice per time point). p.i., postinfection.

(B) Flow cytometric analysis of NK cell activation in cervical lymph nodes 24 hr after earflap infection (mean ± SEM of six lymph nodes per group) is shown.

(C) Flow cytometric analysis of infection index in mice treated with anti-NK1.1 (to deplete NK cells) or an isotype control is shown. Graphs depict infection index in individual mice at days 5–7 after oral infection, normalized to the average of the isotype control-treated mice analyzed on the same day. Error bars represent the mean ± SEM; symbols represent an individual mouse. Data are pooled from two independent experiments.

*p < 0.05. ns, not significant.

Here, we use in vivo infection of mice with the intracellular protozoan parasite, *Toxoplasma gondii*, to address these questions. We previously showed that, following oral or subcutaneous infection, *T. gondii* parasites invade CD169$^+$ macrophages at the lymph node capsule, which can then serve as antigen-presenting cells (APCs) to CD8$^+$ T cells (Chtanova et al., 2008, 2009). In this study we show that NK cells accumulate beneath the lymph node capsule following *T. gondii* infection. Infection also increases the interactions of NK cells with collagen, contributing to a slow and confined migration pattern and accumulation of NK cells near foci of infection beneath the lymph node capsule. We also observe interactions between NK cells and CD169$^+$ macrophages near the lymph node capsule and provide evidence that these cells can regulate NK cell activity. These data provide insight into the in vivo regulation of NK cells and implicate a myeloid population with characteristics of both resident CD169$^+$ subcapsular sinus macrophages and inflammatory monocytes as an important regulator of NK cells during *T. gondii* infection.

RESULTS

Activation and Function of NK Cells in *T. gondii* Infection

We began our studies by examining NK cell responses in mice infected via the physiologically relevant oral route. We infected

mice with tissue cysts of the type II Prugniaud strain engineered to express tdTomato (Chtanova et al., 2008, 2009; Schaeffer et al., 2009). Expression of this fluorescent reporter allows us to monitor infection levels in tissues by flow cytometry, which we convey here as the percentage of infected cells (infection index). Following oral infection, *T. gondii* was first detectable in the draining mesenteric lymph node at 4 days postinfection and continued to increase until at least 7 days postinfection (Figure 1A, upper left). By contrast, *T. gondii* was not detected in spleen until 6 days postinfection. Total numbers (but not proportion) of NK cells were elevated in the mesenteric lymph node until day 6 after infection but did not show a similar increase in the spleen (Figure 1A, upper middle, right). NK cell activation, as measured by CD69 and IFN-γ expression, was readily detectable at day 3 and peaked by day 5 after infection (Figure 1A, lower left and middle). This contrasted to the ex vivo production of IFN-γ by CD3$^+$ T cells that was not detected until day 4 and continued to rise over the course of the experiment (Figure 1A, lower right). These results support the notion that NK cells are an important early source of IFN-γ in *T. gondii* infection (Hunter et al., 1994; Gazzinelli et al., 1993, 1994; Johnson et al., 1993; Denkers et al., 1993).

We recently described a model of *T. gondii* infection in which tachyzoites are injected into the earflap, and the immune response studied in the draining cervical lymph node (Chtanova et al., 2008, 2009). This model provides a synchronous representation of the immune response in the lymph node, important features of which can then be validated in the more

physiologically relevant oral infection model. Using the earflap model, we again observed an increase in NK cell number in the draining cervical lymph node, and these NK cells expressed both CD69 and IFN-γ (Figure 1B). Consequently, we utilized both of these models to assess the relationship between NK cell motility and function in this study.

Previous studies have suggested a protective role for NK cells during *T. gondii* infection; however, many of these studies used depletion methods that could also affect myeloid populations and/or were performed using mice lacking T cell populations (Combe et al., 2005; Denkers et al., 1993; Gazzinelli et al., 1993; Goldszmid et al., 2007; Johnson et al., 1993; Khan et al., 1994, 2006). To confirm the protective role of NK cells under our experimental conditions, we depleted mice of NK cells by administration of NK1.1 antibody. We observed a significant increase in parasite burden in the spleen and mesenteric lymph node 5–7 days after oral infection (Figure 1C). NK cell depletion also led to increased parasite burden in mice of the same strain (C57Bl/6) obtained from a different vendor (The Jackson Laboratory; data not shown). However, in this case the effect was less dramatic, perhaps due to the distinct composition of the intestinal flora, and the related differences in intestinal immune function (Ivanov et al., 2008, 2009). Nevertheless, NK cell activation in response to *T. gondii* was similar in all sources of mice used in this study (data not shown).

NK Cells Accumulate beneath the Lymph Node Capsule following Earflap Infection

We next asked how NK cell distribution in the lymph node changes following *T. gondii* infection. In order to track NK cells, we used mice in which one copy of the *Ncr1* gene (which encodes the NKp46 receptor) had been replaced with a GFP reporter (Gazit et al., 2006). Reporter mice were infected in the earflap with type II Prugniaud tachyzoites expressing tdTomato, and the cervical lymph node was examined 18–24 hr later. Consistent with our previous observations using the type I RH strain, *T. gondii* tachyzoites were concentrated in the region just beneath the lymph node capsule (Chtanova et al., 2008, 2009). Strikingly, large aggregates of NK cells formed just beneath the lymph node capsule in close proximity to foci of infection (Figure 2A). To quantify the relocalization of NK cells upon infection, we used anti-LYVE-1 staining to define the subcapsular sinus and medulla of the lymph node and calculated the density of NK cells in different regions (Figures 2B and 2C). Following infection, NK cell density increased throughout the lymph node, but the increase in density was most dramatic in the subcapsular sinus region (Figure 2C). NK cells could also be detected beneath the capsule of the mesenteric lymph node following oral infection, although in this case relocalization of the cells was less dramatic (Figure 2D).

NK Cells Interact with Collagen Fibers in Infected Lymph Nodes

Two-photon laser-scanning microscopy (TPLSM) of cervical and mesenteric lymph nodes revealed that a portion of NK cells in the subcapsular region of the lymph node exhibited a relatively slow, confined migration pattern (Figure 2E; Movie S1). The confined migration pattern suggested that NK cells might be interacting

with an immobile structure in the lymph node. Indeed, we observed that a substantial fraction of the slow-moving NK cells closely associated with second harmonic signals indicative of collagen fibers (Figure 3A; Movie S2). Antibody staining of lymph node tissue sections confirmed that these structures contained type I collagen (Figure 3B). Interactions between NK cells and collagen took place at the lymph node capsule and along fiber-like structures extending away from the capsule (data not shown). Collagen interactions occurred with individual NK cells, and with stable swarms of NK cells focused around a central structure with a prominent second harmonic signal (Figure 3C; Movie S3).

If the slow, confined migration pattern of NK cells reflects their interaction with collagen fibers, we would expect to observe a correlation between speed and proximity to collagen within TPLSM imaging volumes. To test this, we calculated the distance between individual NK cells and the collagen capsule, and plotted this distance against NK cell speed (Figure 3D). In infected lymph nodes the slowest NK cells tended to be located close to collagen. Interestingly, this correlation was not seen in lymph nodes from uninfected mice, suggesting that changes related to infection promoted the association between NK cells and collagen in cervical lymph nodes (Figure 3D; p < 0.0001).

Collagen Interactions Promote NK Cell Accumulation in Foci of Infection near the Lymph Node Capsule

The interaction between NK cells and collagen fibers raised the question of which receptors might be involved in this interaction, and how it may regulate NK cell motility. NK cells express CD49b (α2-integrin), which can act as a receptor for collagen when paired with the β1-integrin chain (Arase et al., 2001; Miyake et al., 1994; White et al., 2004). We therefore investigated the impact of blocking antibodies to CD49b on NK cells during infection (Miyake et al., 1994). Twenty hours after earflap infection, anti-CD49b (clone HMα2) or an isotype control antibody was delivered into the earflap. After a further 4 hr, cervical lymph nodes were analyzed by TPLSM. Administration of blocking antibody resulted in a reduction in the percentage of NK cells that fell within the slow-moving confined population (average speed <5 μm/min, red tracks) (Figure 3E; Movie S4). We also observed a reduction in NK cell density within foci of infection near the lymph node capsule (Figures 3F, 3G, and S1). Antibody treatment at the time of infection did not lead to a significant change in CD69 or IFN-γ expression by NK cells (data not shown). These data indicate that interactions between CD49b on NK cells and collagen fibers in the lymph node, whereas not essential for NK cell activation, may serve to retain NK cells near their sites of action in the lymph node.

NK Cells Interact with CD169+ Cells at the Subcapsular Sinus

A portion of NK cells with slow, confined migration is present even after blocking the CD49b-collagen interaction, suggesting that the NK cells engage in another type of interaction in this location. CD169+ macrophages lining the subcapsular sinus of the lymph node are a target for *T. gondii* (Chtanova et al., 2008); therefore, we examined the migration of NK cells relative to CD169+ cells by injecting fluorescent antibody to CD169 just
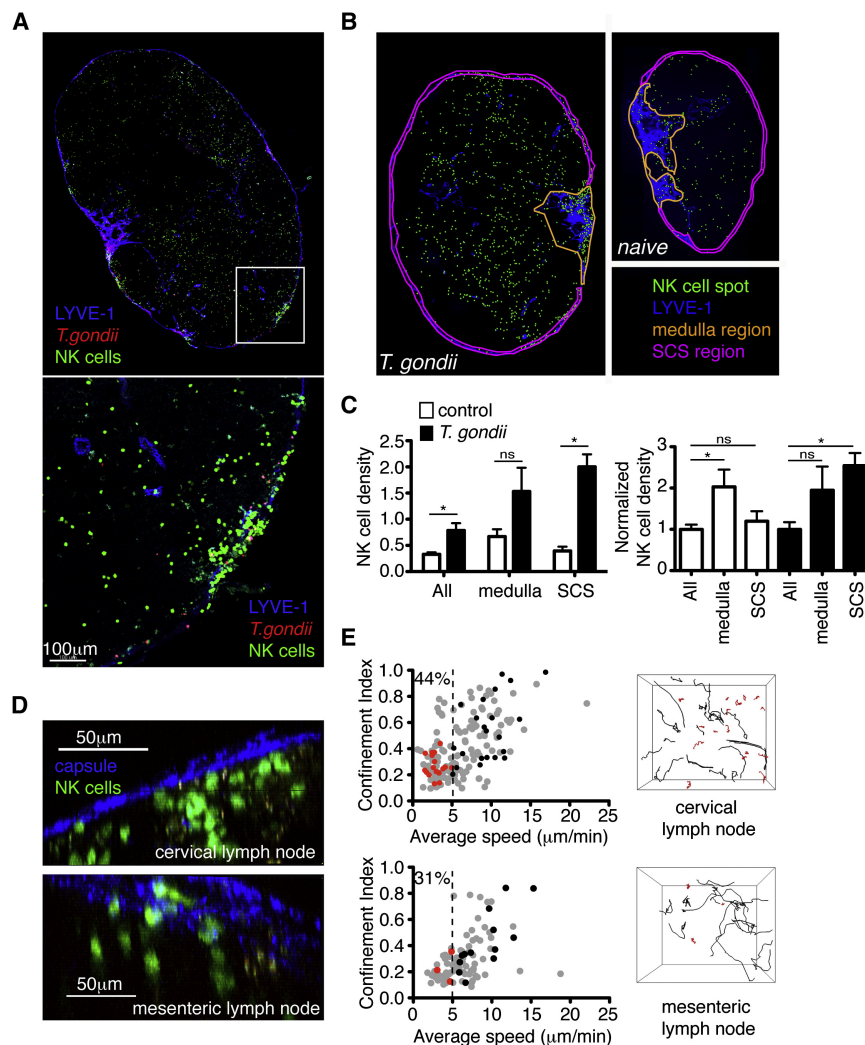
Figure 2. NK Cells Accumulate beneath the Lymph Node Capsule following *T. gondii* Infection and Fall into Two Populations with Distinct Motility

(A) Confocal analysis of the cervical lymph node from an *Ncr1*^GFP/+ mouse 24 hr after earflap infection is shown. NK cells are green, *T. gondii* is red, and LYVE-1 staining of lymphatic vessels is blue. The top panel shows a map of an entire lymph node section, whereas the bottom panel is a close-up view of the boxed region.

(B and C) Analysis of NK cell density in different regions of the lymph node is illustrated. (B) Maps of cervical lymph nodes from *Ncr1*^GFP/+ mice acquired by epifluorescence microscopy in the absence of infection (right), and 18–24 hr after earflap infection (left) are presented. NK cell spots are green, LYVE-1 staining is blue, and regions corresponding to the medulla or subcapsular sinus (SCS) are outlined in yellow and pink, respectively. (C) Graphs depict NK cell density (left) and NK cell density normalized to the average NK cell density across the whole uninfected or infected lymph node (right). Error bars depict the mean ± SEM of five lymph nodes analyzed for each of the control (white bars) and infected (black bars) groups. Data are pooled from three independent experiments. *p < 0.05.

(D) TPLSM analysis of lymph nodes from *Ncr1*^GFP/+ mice 24 hr after earflap infection (top) and 4 days after oral infection (bottom) is shown. Second harmonic generation from the lymph node capsule is in blue, and NK cells are green.

(E) TPLSM analysis of lymph nodes from *Ncr1*^GFP/+ mice 18–24 hr after earflap infection (top panels, corresponds to Movie S1) or 5 days after oral infection (bottom panels) is illustrated. Graphs show the average speed and confinement index (maximum displacement/path length) of individual NK cells. For each condition data are pooled from imaging runs obtained from at least two independent experiments. Numbers indicate the percentage of NK cells migrating at <5 μm/min. Data from an individual run are highlighted in red (cells migrating at <5 μm/min) and black (cells migrating at >5 μm/min). These correspond to the tracks of individual NK cells shown in the right-hand panels.

prior to analysis by TPLSM. NK cells formed interactions with CD169+ cells, and these often occurred with CD169+ cells that did not contain any visible parasite fluorescence (Figure 4A; Movie S5). The duration and type of interactions formed between CD169+ cells and NK cells varied markedly between imaging volumes, but we often observed interactions that persisted for the duration of the imaging run (>19 min) (Figure 4B; Movie S5). Persistent interactions between NK cells and CD169+ cells were also observed in uninfected lymph nodes, but far fewer NK cells were present in the subcapsular region of the lymph node at this time (Figure 4B). We confirmed the existence of interactions between NK cells and CD169+ cells by staining sections from infected cervical lymph node and mesenteric lymph node with an antibody to CD169. Again, this revealed close contacts between NK cells and CD169+ cells near the lymph node capsule (Figure 4C).

We previously noted disruption of the CD169+ cell layer in *T. gondii*-infected lymph nodes, which was driven in part by the activity of neutrophils swarming near foci of infection (Chtanova et al., 2008). Consistent with this, TPLSM of uninfected lymph nodes revealed networks of CD169+ cells with dendritic morphology, whereas infected lymph nodes contained areas in which the CD169+ cell layer no longer appeared continuous, and the morphology of the cells was more rounded (Figure 4D). We compared the density of NK cells in regions with an intact network of CD169+ cells to regions in which the CD169+ cells had altered morphology. NK cell density was higher in regions in which the CD169 layer appeared disrupted, suggesting that local remodeling of the region gives access to NK cells (Figure 4D; Movies S6, S7, and S8). This is reminiscent of the recent finding that the arrival of mature tissue DCs in the subcapsular sinus results in morphological changes to the subcapsular sinus floor, opening up an additional point of access for afferent lymph-derived T cells (Braun et al., 2011).

The heterogeneous morphology of CD169+ cells in infected lymph nodes prompted us to analyze the composition of this
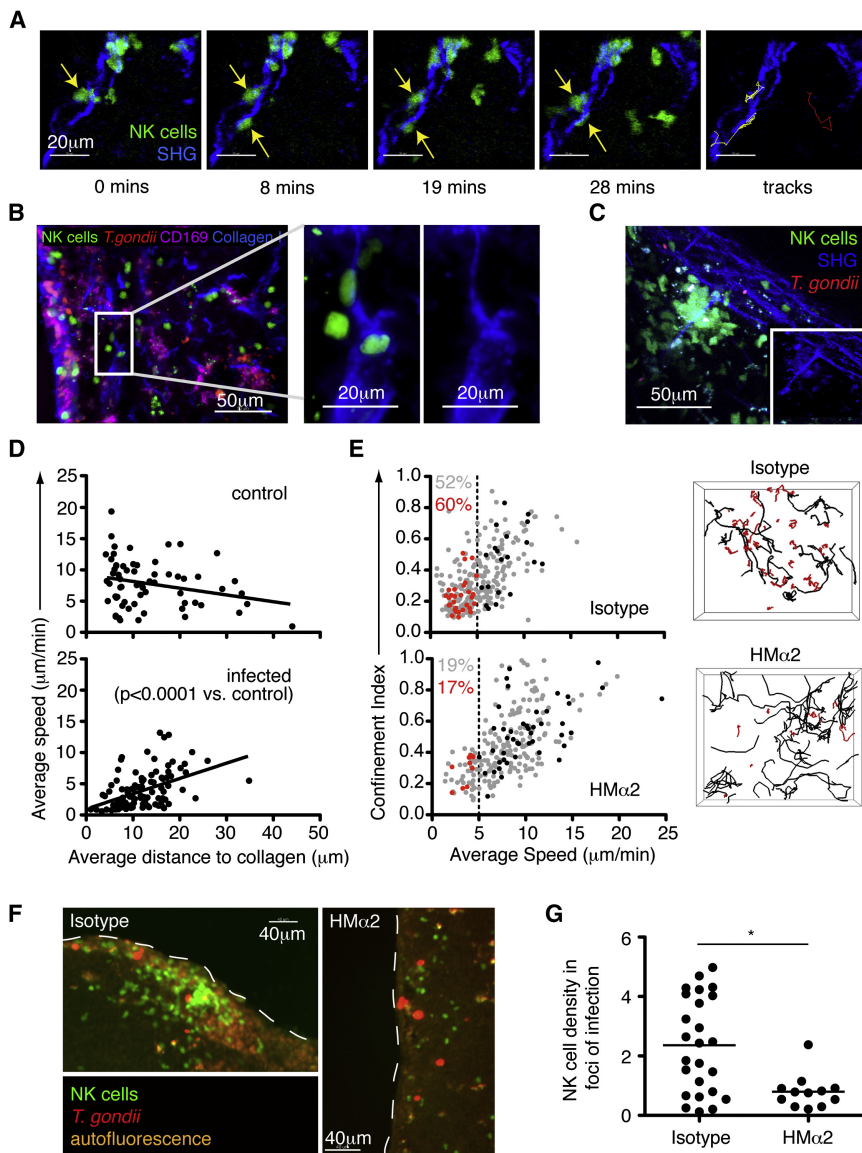
Figure 3. Collagen Interactions Promote NK Cell Accumulation in Foci of Infection near the Capsule of Infected Cervical Lymph Nodes

(A) Individual time points and tracks from a TPLSM movie showing two NK cells (green, yellow tracks) interacting with a collagen fiber (second harmonic [SHG], blue) in the cervical lymph node 24 hr after earflap infection are presented. The track of an NK cell that does not interact with collagen is shown for comparison (red). Corresponds to Movie S2.

(B) Analysis of cervical lymph nodes 24 hr after earflap infection by epifluorescence microscopy is shown. CD169 staining is shown in purple, collagen type I staining in blue, NK cells in green, and *T. gondii* in red. The panels on the right are close-up views of the boxed region.

(C) Still image from a TPLSM movie showing a stable swarm of NK cells (green) centered around a collagen fiber (second harmonic, blue) is illustrated. Inset image is from the same movie but with NK cell signal removed. Corresponds to Movie S3.

(D) TPLSM analysis comparing the average speed of NK cells to their average distance to the nearest collagen (second harmonic) structure over the course of an imaging run is shown. Each data point represents an individual NK cell.

(E) TPLSM analysis of NK cell motility in cervical lymph nodes from *Ncr1*[GFP/+] mice infected in the earflap with *T. gondii* 24 hr previously, and administered anti-CD49b (clone HMα2) or an isotype control 4 hr previously is presented. Graphs show the average speed and confinement index of individual NK cells. For each condition data are pooled from four imaging runs obtained from at least two independent experiments. The average imaging depth for HMα2-treated nodes was 57.5 μm, and 61.5 μm for isotype-treated nodes. All movies contained the lymph node capsule as a point of reference. Data from an individual run are highlighted in red (cells migrating at <5 μm/min) and black (cells migrating at > 5 μm/min). These correspond to the tracks of individual NK cells shown in the right-hand panels. Numbers indicate the percentage of NK cells migrating at <5 μm/min (red for highlighted imaging run, and gray for all imaging runs depicted). Corresponds to Movie S4.

(F and G) Epifluorescence analysis of cervical lymph nodes from *Ncr1*[GFP/+] mice 24 hr after earflap infection with *T. gondii* tachyzoites and administration of HMα2 or an isotype control is illustrated. (F) Images show foci of infection beneath the lymph node capsule. NK cells are in green and *T. gondii* in red. Dashed line denotes lymph node capsule. (G) Graph depicts NK cell density within foci of infection. Each data point represents a single focus of infection. Data are pooled from two independent experiments, representing a total of six isotype-treated and four HMα2-treated lymph nodes. Bars represent the mean. *p < 0.05. Corresponds to Figure S1.

---

population by flow cytometry (Figure 5A). In uninfected lymph nodes the CD169^{+} population could be divided into CD11c^{high} and CD11c[low/int] subpopulations, which likely represent a portion of the conventional DC population and sinusoidal (subcapsular sinus or medullary) macrophages, respectively (Figure 5A) (Phan et al., 2009). The CD169^{+}CD11c[low/int] macrophage population expressed CD11b and low-to-intermediate levels of Ly6C. Following infection an additional population of CD11b^{high} Ly6C^{high} cells appeared among the CD169^{+}CD11c[low/int] population (Figures 5A and 5B). This population of CD169^{+}Ly6C^{high} cells

was almost completely absent in the steady state but increased dramatically in proportion and absolute number following infection (Figure 5B). The pattern of CD11b and Ly6C expression on these cells was reminiscent of inflammatory monocytes. We therefore looked for expression of other inflammatory monocyte-associated markers. A comparable or increased proportion of CD169^{+}Ly6C^{high} cells expressed CCR2, iNOS, and Ly6B2 as compared to the CD169^{−}Ly6C^{high} inflammatory monocyte population (Figures 5B, 5C, and S2). Because CD169^{+}Ly6C^{high} cells shared features of both inflammatory monocytes and
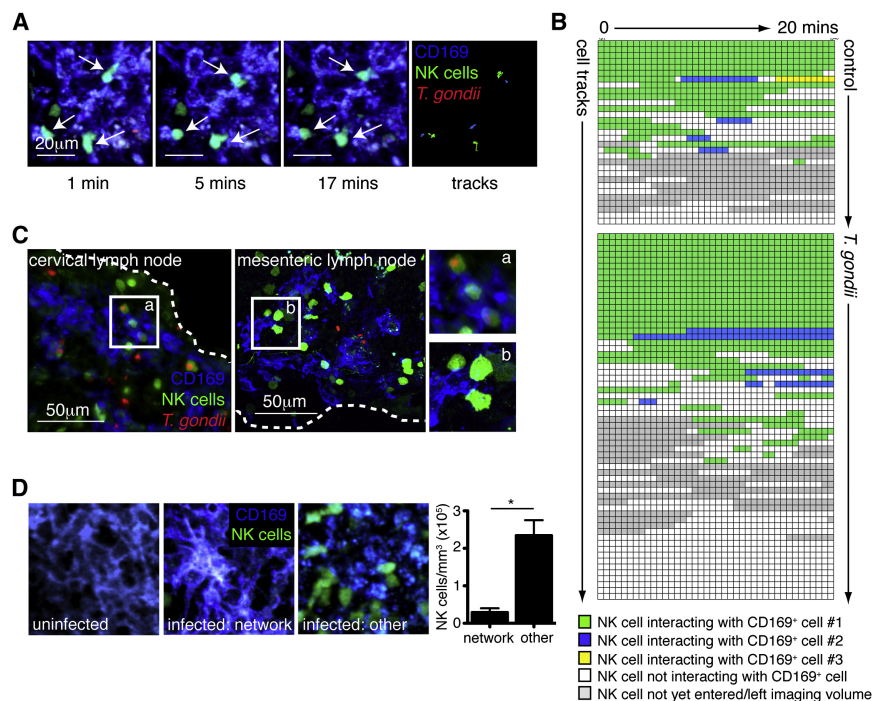
Figure 4. NK Cells Interact with CD169⁺ Cells in the Subcapsular Region of the Lymph Node

(A) Individual time points and tracks from a TPLSM movie showing three NK cells (green) forming prolonged interactions with CD169⁺ cells (blue) in the cervical lymph node 24 hr after earflap infection are shown. Corresponds to Movie S5.

(B) Analysis of interactions between NK cells and CD169⁺ cells is shown. Each row represents an NK cell, and each box represents a single time point of approximately 30 s. Green boxes indicate a close interaction between an NK cell and CD169⁺ cell, and blue and yellow boxes indicate interactions with second or third CD169⁺ cells, respectively. Analysis of two to three imaging runs from two independent experiments are shown for each condition. Only NK cells outside of swarms were analyzed.

(C) Epifluorescence or confocal analysis of cervical lymph nodes and mesenteric lymph nodes harvested 24 hr after earflap infection and 5 days after oral infection, respectively, is presented. Dashed white lines indicate the position of the lymph node capsule. The panels on the right are close-up views of the boxed regions with corresponding labels.

(D) TPLSM analysis of cervical lymph nodes is shown. Images are from a single time point and show CD169⁺ cells (blue) and NK cells (green). The graph shows the density of NK cells in regions of infected lymph node with an intact network of CD169⁺ cells ("network") and in other subcapsular regions exhibiting CD169 staining ("other"). Error bars represent mean ± SEM. *p < 0.05. Corresponds to Movies S6, S7, and S8.

subcapsular sinus macrophages, we refer to them here as CD169⁺Ly6C^high inflammatory macrophages.

To determine if CD169⁺Ly6C^high inflammatory macrophages contact NK cells in the subcapsular region of the lymph node, we stained sections with antibodies to Ly6B2 (expressed by neutrophils and inflammatory monocytes/macrophages) and Ly6G (expressed by neutrophils) (Kang et al., 2008). Ly6B2⁺Ly6G⁻ cells were seen in aggregates beneath the lymph node capsule, and a subpopulation of Ly6B2⁺Ly6G⁻ cells also stained with an antibody to CD169 (Figure 5D). NK cells were seen in close contact with both CD169⁺Ly6B2⁻Ly6G⁻ cells (CD169⁺ subcapsular sinus macrophages) and CD169⁺Ly6B2⁺Ly6G⁻ cells (CD169⁺Ly6C^high inflammatory macrophages) (Figure 5D).

Reduced NK Cell Activation following Treatment with Clodronate Liposomes

We next investigated the effect of in vivo depletion of phagocytic cells in the subcapsular sinus on NK cell activation. Mice were treated with clodronate or PBS encapsulated in liposomes via the earflap route, and infected with *T. gondii* tachyzoites 8–9 days later. Subcutaneous injection of liposome-encapsulated clodronate led to local depletion of both CD169⁺ subcapsular sinus macrophages (CD169⁺CD11b⁺CD11c^low/int Ly6C^low/int) and CD169⁺Ly6C^high inflammatory macrophages (CD169⁺CD11b^high CD11c^low/int Ly6C^high) in the draining lymph node (Figure 6A). Notably, depletion of the CD169-expressing subpopulations was much more dramatic than depletion of either the CD11b⁺CD11c^low/int Ly6C^low/int or CD11b⁺CD11c^low/int Ly6C^high

populations as a whole. Similarly, the proportion of CD11c^high cells remained unchanged, whereas we observed a slight reduction in CD169⁺CD11c^high cells (Figure 6A). This preferential depletion of CD169-expressing populations may result from delivery of liposomes through the lymphatics, leading to selective depletion of myeloid cells present in the subcapsular region of the lymph node. Although the overall proportion of NK cells and the level of infection were not altered by liposome-encapsulated clodronate treatment, the proportion of NK cells expressing CD69 and IFN-γ was significantly reduced (Figures 6B and 6C).

NK Cells Can Be Activated by CD169⁺Ly6C^high Inflammatory Macrophages

To confirm a role for CD169⁺ macrophages in NK cell activation, we isolated CD169⁺CD11b⁺CD11c^low/int macrophages from the mesenteric lymph nodes of uninfected or orally infected mice and cultured them in vitro with NK cells isolated from uninfected mice (Figure 7A). CD169⁺/⁻CD11b⁺CD11c^high DCs served as a comparison control for NK cell activation. Coculture with CD169⁺CD11b⁺CD11c^low/int cells from infected mice resulted in NK cell activation, as assessed by expression of CD69 and IFN-γ (Figures 7B and 7C). Surprisingly, this activation was even more robust than what was observed in the presence of DCs (Figure 7B). NK cell activation was far less dramatic when NK cells were cultured in the presence of CD169⁺CD11b⁺CD11c^low/int cells or DCs isolated from uninfected lymph nodes (Figure 7B).

Having established that CD169⁺CD11b⁺CD11c^low/int lymph node cells from infected mice are capable of activating NK cells,
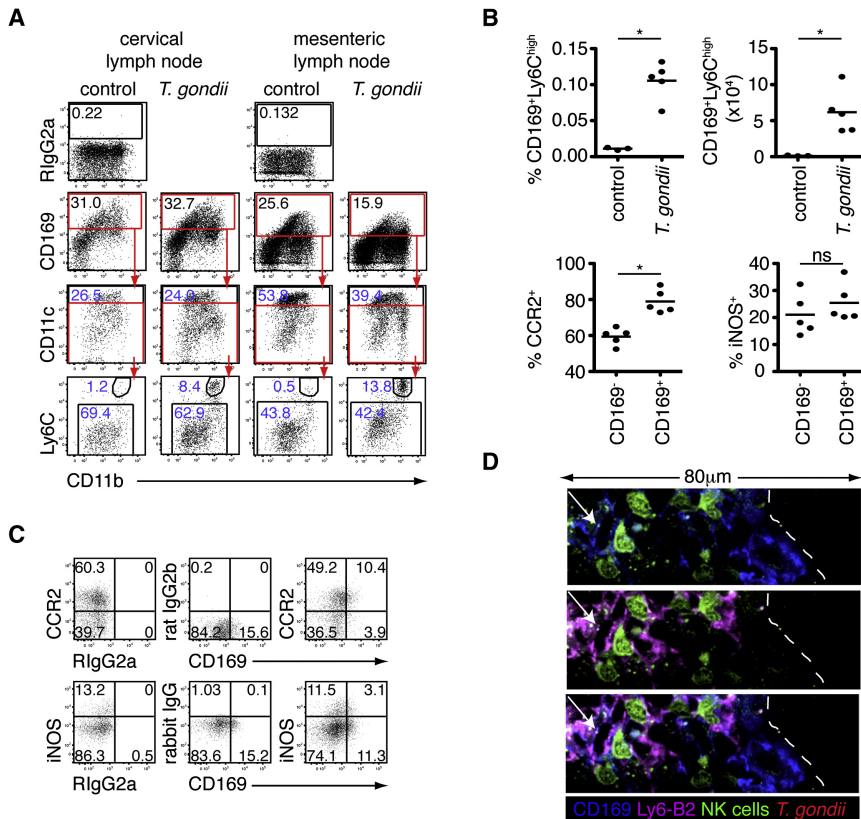
Figure 5. Altered Composition of the CD169+ Cell Population in *T. gondii*-Infected Lymph Nodes

(A) Flow cytometric analysis of CD169+ cells in the lymph node following earflap (6 hr) or oral (5 days) infection (dead cells, T cells, B cells, NK cells, and neutrophils excluded) is shown. Plots show gating of CD169+ cells into CD11c^{high} and CD11c$^{low/int}$ populations, and gating of CD169+CD11c$^{low/int}$ cells into Ly6C^{high}CD11b^{high} and Ly6C^{low}CD11b^{+} populations. Numbers in blue indicate the percentage of the gated cell population among all CD169+ cells.

(B and C) Flow cytometric analysis of CD169+Ly6C^{high} cells in mesenteric lymph nodes 5 days after oral *T. gondii* infection is presented. (B) Top panels show the proportion and absolute number of CD169+Ly6C^{high} cells in uninfected and *T. gondii*-infected lymph nodes. Bottom panels depict the proportion of CD169+Ly6C^{high} cells expressing CCR2 or iNOS. Bars represent the mean. (C) Representative flow plots (see also Figure S2) are shown. *p < 0.05.

(D) Confocal analysis of cervical lymph nodes 24 hr after earflap infection is presented. CD169 staining is in blue and Ly6-B2 in pink. No Ly6G+ cells are shown in this image. NK cells are shown in green. A CD169+ inflammatory macrophage (arrow) is seen interacting with an NK cell beneath the lymph node capsule (dashed line).

we further subdivided this population based on expression of Ly6C (Figure 7D). Increased expression of CD69 and IFN-γ was most dramatic following culture with CD169+Ly6C^{high} inflammatory macrophages, demonstrating that these cells are capable of activating or priming the NK cell response during *T. gondii* infection (Figures 7E and 7F). These data do not exclude the possibility that other cell types, including DCs, may contribute to NK cell activation in vivo. Nevertheless, the potency of CD169+Ly6C^{high} inflammatory macrophages isolated from infected lymph nodes to activate NK cells in vitro, together with the impact of clodronate liposome depletion on in vivo NK cell activation, and the extensive contacts between NK cells and CD169+ cells observed in vivo, strongly points to a role for these interactions in activation of NK cells during in vivo infection.

DISCUSSION

During infection NK cells must interact with other cells in order to become fully activated and to carry out their effector functions. However, we have limited information about how this occurs in vivo. Here, we used a *T. gondii*-mouse infection model in conjunction with TPSLM to address this question. We found that NK cells accumulate in the subcapsular region of the lymph node near foci of infection, where they engage in relatively stable interactions with CD169+ cells. Infection also promotes the association of NK cells with collagen fibers near the lymph node

capsule, thereby promoting accumulation of NK cells near foci of infection. Our results provide an anatomical and dynamic context for understanding NK cell responses during infection and provide evidence for a role for myeloid cells in the subcapsular sinus of the lymph node in NK cell activation.

Our results contribute to a growing body of evidence that the subcapsular region of the lymph node, and the CD169+ macrophages found there, play a crucial role in the initiation of immune responses. Macrophages at the subcapsular sinus have been previously implicated in transportation and presentation of antigen to B cells, antigen presentation for conventional T cells and invariant NK T cells, and production of type I IFN following viral infection (Carrasco and Batista, 2007; Barral et al., 2010; Chtanova et al., 2009; Iannacone et al., 2010; Junt et al., 2007; Phan et al., 2007, 2009). Interestingly, the CD169+ population in infected lymph nodes with the greatest ability to activate NK cells also shares some cell surface markers with inflammatory monocytes, leading us to call these cells CD169+Ly6C^{high} inflammatory macrophages. It is possible that CD169+Ly6C^{high} inflammatory macrophages derive from the CD169+ macrophage population resident in the subcapsular sinus of the resting lymph node. However, we favor the possibility that they are derived from inflammatory monocytes, a cell type previously shown to play a protective role in *T. gondii* infection (Dunay et al., 2008). Inflammatory monocytes that are recruited to the subcapsular region of the lymph node may upregulate CD169 as a response to the local tissue environment or may acquire the antigen via
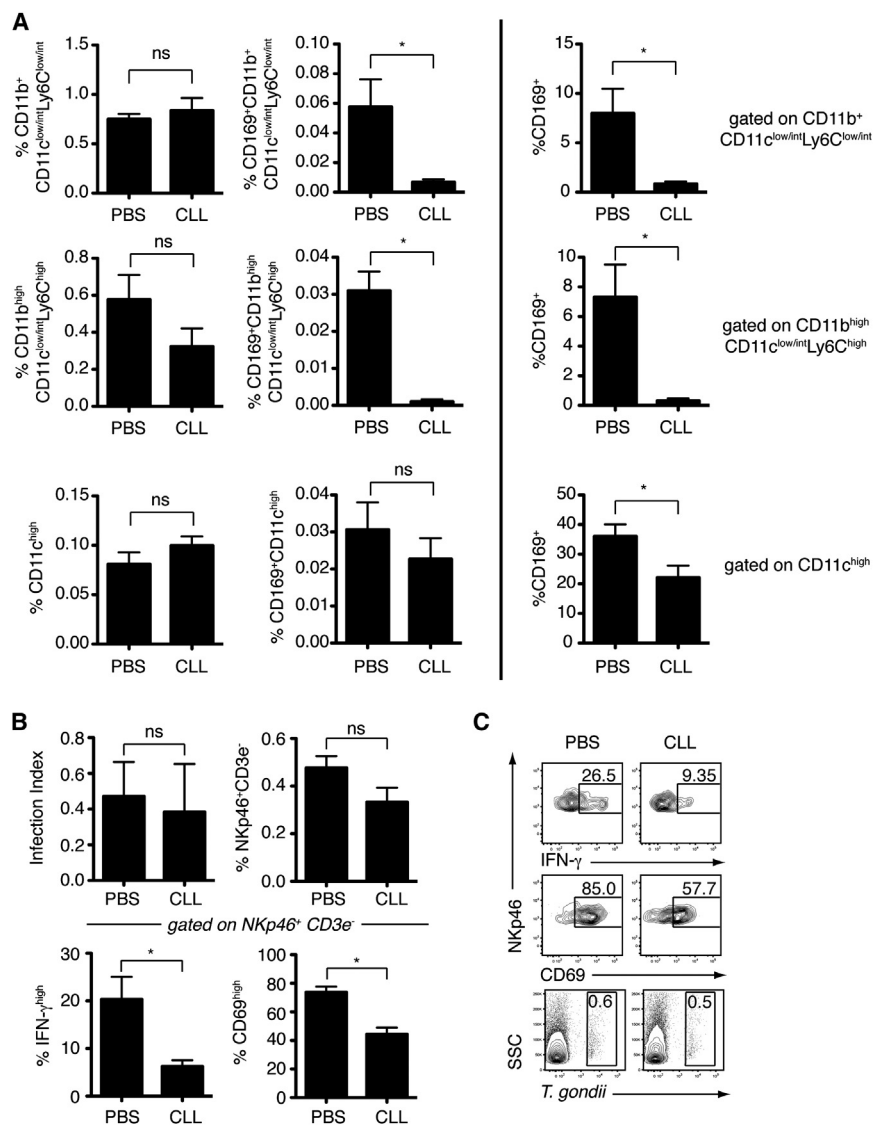
Figure 6. Reduction in NK Cell Activation following Treatment with Liposome-Encapsulated Clodronate

Flow cytometric analysis of cervical lymph nodes from mice treated with liposome-encapsulated clodronate (CLL) or PBS, and infected in the earflap with *T. gondii* is shown.

(A) Flow cytometric analysis of myeloid cell populations is shown. Analysis was performed on cells negative for lineage markers (TCRαβ, CD19, NKp46) and Aqua Live/Dead stain. For the top two rows, cells were also gated as CD11c$^{low/int}$. Top row (left to right) depicts overall percentage of CD11b$^+$CD11c$^{low/int}$Ly6C$^{low/int}$ cells and CD169$^+$CD11b$^+$CD11c$^{low/int}$Ly6C$^{low/int}$ cells (sinusoidal macrophages) and percentage CD169$^+$ cells among CD11b$^+$CD11c$^{low/int}$Ly6C$^{low/int}$ cells. Middle row (left to right) depicts overall percentage of CD11b^{high}CD11c$^{low/int}$Ly6C^{high} cells (inflammatory monocytes/macrophages) and CD169$^+$ CD11b^{high}CD11c$^{low/int}$Ly6C^{high} cells (CD169$^+$Ly6C^{high} inflammatory macrophages) and percentage CD169$^+$ cells among CD11b^{high}CD11c$^{low/int}$Ly6C^{high} cells. Bottom row (left to right) depicts overall percentage of CD11c^{high} cells and CD169$^+$CD11c^{high} cells and percentage CD169$^+$ cells among CD11c^{high} cells. Data are from one representative experiment of two performed and represent six nodes analyzed for each group.

(B) Flow cytometric analysis of infection index, percentage of NKp46$^+$CD3ε$^-$ cells among live cells, percentage of CD69$^+$ cells among NKp46$^+$CD3ε$^-$ cells, and percentage of IFN-γ$^+$ cells among NKp46$^+$CD3ε$^-$ cells is shown. NK cells were identified by GFP expression or staining with anti-mouse NKp46 antibody. Data are pooled from two independent experiments and represent ten nodes analyzed for each infected group.

(C) Representative flow cytometry plots are shown. Error bars represent the mean ± SEM. *p < 0.05.

transfer from resident CD169-expressing macrophages (Gray et al., 2012). In this context the CD169 marker may indicate activation or exposure to an inflammatory environment, rather than serving as a marker for resident subcapsular macrophages (Biesen et al., 2008).

Although a variety of cell types are capable of acting as accessory cells for NK cell activation in vitro, many in vivo studies have focused on the role of DCs, leaving the in vivo role of macrophages and monocytes relatively underexplored (Andrews et al., 2003; Fernandez et al., 1999; Hou et al., 2011; Kassim et al., 2006; Lucas et al., 2007; Pribul et al., 2008; Schleicher et al., 2007). It is likely that the relative contributions of DCs, macrophages, and monocytes in vivo will vary with the route and type of infection. For example production of IFN-γ by splenic NK cells in response to intraperitoneal *T. gondii* infection is impaired in Batf3$^{-/-}$ mice, which lack CD8$^+$ DCs (Mashayekhi et al., 2011). Furthermore, NK cells formed prolonged contacts with DCs in *Leishmania major*-infected lymph nodes (Bajénoff

et al., 2006). Although we also found that DCs isolated from mesenteric lymph nodes following oral *T. gondii* infection could activate NK cells in vitro, they were less efficient at inducing IFN-γ production compared to CD169$^+$CD11c$^{low/int}$ macrophages.

Interactions between immune cells and components of the extracellular matrix contribute to the spatial organization and regulation of the immune response; however, little is know about how these interactions change during infection. Here, we identified an important role for the interaction between CD49b and collagen for regulation of NK cell migration in vivo during infection. This builds on an earlier study showing that the crosslinking of CD49b that occurs during bead-based sorting of NK cells can alter their motility upon subsequent in vivo transfer (Garrod et al., 2007). In the lymph node, collagen is a major constituent of the lymph node capsule and also forms the core of a network of reticular fibers that extend out from high endothelial venules to the sinuses. The association of NK cells with conduit-associated
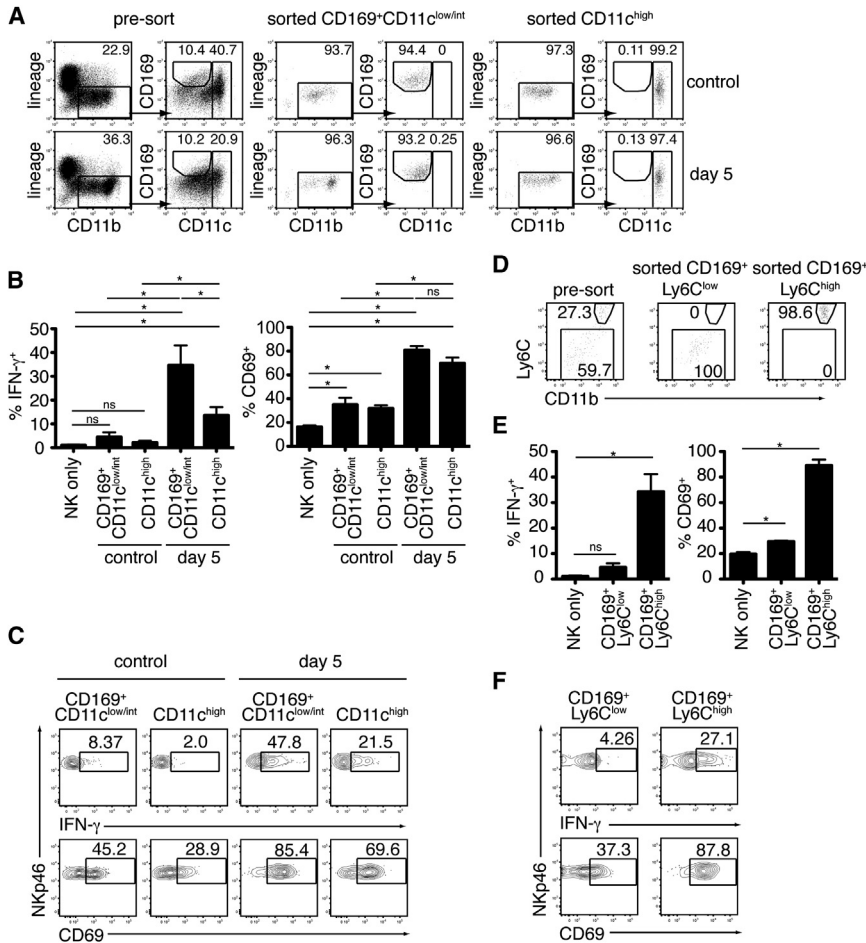
A

B

C

D

E

F

Figure 7. Activation of NK Cells by CD169⁺ CD11b^high CD11c^low/int Ly6C^high Cells in an In Vitro Assay

(A–C) Flow cytometric analysis of NK cell activation following overnight culture with CD11c^high DC or CD169⁺CD11b⁺CD11c^low/int cells sorted from uninfected or day 5 infected mesenteric lymph nodes is shown. (A) Gating strategy and purity of sorted myeloid cell populations are shown. (B) Percentage of NKp46⁺ NK cells expressing IFN-γ and CD69 is presented. Data are pooled from three independent experiments. (C) Representative flow cytometry plots are shown.

(D–F) These are the same as for (A)–(C) but comparing CD169⁺CD11b^high CD11c^low/int Ly6C^high inflammatory macrophages to CD169⁺CD11b⁺ CD11c^low/int Ly6C^low/int macrophages. Myeloid cells were first gated as lineage⁻ CD11b⁺CD169⁺, as in (A).

Error bars represent the mean ± SEM. *p < 0.05.

collagen was somewhat surprising given that in the resting lymph node, it is thought that the collagen core of the reticular fibers is completely ensheathed by fibroblastic reticular cells and, therefore, inaccessible to NK cells (Roozendaal et al., 2008). We speculate that during inflammation-induced remodeling of the lymph node, the pace of collagen deposition may outstrip the rate at which fibers are ensheathed, granting the NK cells access. According to this notion, infection-induced changes in the lymph node that expose collagen could serve as a kind of "danger signal," leading to altered leukocyte trafficking. Increased surface expression or adoption of the high-affinity conformation of the integrin in response to chemokines may also contribute to altered trafficking. Although blocking the CD49b-collagen interaction did not impair NK cell activation in this setting, it did significantly reduce the accumulation of NK cells near foci of infection. Thus, the collagen association may help position activated NK cells close to relevant target cells, thereby aiding in the productive delivery of cytokines and other effector responses within the lymph node. It is also possible that the interaction between NK cell and collagen may contribute to NK cell activity in other settings by fine-tuning the response or by retaining NK cells in a region of the lymph node where they can receive other activating signals.

The recruitment of NK cells into discrete inflammatory foci can facilitate interactions with cells or environments necessary for both their activation and effector function. In an elegant demonstration of this concept, NK cell IFN-γ production in response to *Listeria monocytogenes* infection was shown to be dependent on their recruitment to inflammatory clusters in the spleen, where they promoted the differentiation of inflammatory monocytes into TipDCs (Kang et al., 2008). We have shown previously that infection of CD169⁺ subcapsular sinus macrophages by *T. gondii* results in the formation of neutrophil swarms beneath the lymph node capsule, which contribute to the local remodeling of the CD169⁺ cell layer (Chtanova et al., 2008). Our observation that NK cell-macrophage interactions occur in regions of the capsule where the macrophage layer is disordered suggests that remodeling of the lymph node capsule may facilitate the access of NK cells to CD169⁺ cells. Remodeling at foci of infection may also contribute to CD8⁺ T cell responses because these cells are also recruited to foci of infection and form antigen-specific interactions with CD169⁺ cells (Chtanova et al., 2009). In this way the spatial and temporal pattern of immune cell recruitment to sites of infection may orchestrate the interactions required for optimal generation of immune responses.

An interesting question will be whether this environment can also promote interactions required for NK cell effector function. NK cells can promote macrophage killing of *T. gondii*, and they are implicated in optimizing the T cell response to *T. gondii*, either directly or by increasing IL-12 production by APCs (Combe et al., 2005; Goldszmid et al., 2007; Guan et al., 2007; Hou et al., 2011). Activation of NK cells accumulating near foci of infection in the subcapsular sinus may allow for simultaneous encounters with accessory cells, infected cells, APCs, and

T cells (Klezovich-Bénard et al., 2012). Interactions formed between these cells and NK cells may contribute to control of infection and the generation of an adaptive immune response.

In summary our data support the notion that the subcapsular sinus represents an important site for the initiation of immune responses, provide evidence that macrophages in this region can promote NK cell activity, and reveal a role for collagen interactions in directing NK cells to foci of infection within the lymph node.

EXPERIMENTAL PROCEDURES

Mice

C57Bl/6 mice were purchased from The Jackson Laboratory or Taconic or were bred in-house. Taconic mice were used only in Figure 1C. CBA/J mice were purchased from The Jackson Laboratory. $Ncr1^{GFP/+}$ mice were a gift from Dr. O. Mandelboim (The Hebrew University of Jerusalem) (Gazit et al., 2006). Mice were housed under specific pathogen-free conditions at the AALAC-approved animal facility in the Life Science Addition, University of California, Berkeley. Animal experiments were approved by the Animal Care and Use Committee of University of California, Berkeley.

T. gondii Infections

Type II Prugniaud parasites engineered to express tdTomato and ovalbumin (Chtanova et al., 2008, 2009; Schaeffer et al., 2009) were used for all experiments described. For oral infections, 50 cysts isolated from the brains of chronically infected mice were administered by gavage. For earflap infections, 1×10^6 tachyzoites isolated from in vitro cultures were injected per earflap.

Depletion of NK Cells

Mice were given 250 μg anti-NK1.1 (PK-136) or a rat IgG2a isotype control (UCSF Hybridoma and Monoclonal Antibody Core) i.p. 1 day prior to and 3 days after oral infection. Depletion of NK cells was confirmed by staining single-cell suspensions of mesenteric lymph node and spleen with antibodies to NKp46 (29A1.4; eBioscience) and CD3ε (145-2C11; eBioscience).

Confocal/Epifluorescence Image Analysis

For quantification of NK cell density, NK cells were enumerated by applying spots to each NK cell using Imaris software. LYVE-1 staining was used to define regions corresponding to the medulla or subcapsular sinus in ImageJ. Alternatively, foci of infection at the lymph node capsule were identified, and a region extending 60 pixels beneath the lymph node capsule was drawn using ImageJ. The areas of these regions were determined using ImageJ, and the density of NK cells within each region was calculated. Analysis of infected cell density was performed in the same way.

Two-Photon Imaging

Two-photon imaging was performed on lymph nodes that had been explanted and perfused in warmed oxygenated media, as previously described by Bousso and Robey (2003). Cervical lymph nodes were prepared for imaging 18–24 hr after earfap infection, and mesenteric lymph nodes 4–5 days after oral infection. All imaging experiments were performed using $Ncr1^{GFP/+}$ mice. In some experiments, 10 μg anti-CD49b (HMa2; eBioscience) or isotype control was injected into the earflap 4 hr prior to imaging. In other experiments, 10 μl neat in-house AF532-labeled anti-CD169 antibody (AbD serotec) was injected into the earflap just prior to sacrifice. Further technical details are provided in the Extended Experimental Procedures.

To evaluate the relationship between NK cell speed and proximity to collagen, we tracked the position of each NK cell over time using Imaris and then defined the location of the collagen at each time point by generating an isosurface based on the second harmonic signal (Gaussian, 0.5; threshold, 45), and filling the entire "collagen isosurface" with 1 μm diameter "collagen spots." For each NK cell at each time point, we calculated its distance to the nearest collagen spot and its interval speed based on the position of the same NK cell in the successive time point. Data are presented as the average of distance to closest collagen spot versus average of interval speed for each NK cell track.

In Vivo Depletion of Macrophages

Mice were injected in the earflap with a suspension of clodronate or PBS-loaded liposomes 8–9 days prior to infection. Clodronate was encapsulated in liposomes as described previously by Van Rooijen and Sanders (1994). Phosphatidylcholine (LIPOID E PC) was obtained from Lipoid GmbH, Ludwigshafen, Germany. Cholesterol was purchased from Sigma-Aldrich, St. Louis. Clodronate was a gift of Roche Diagnostics GmbH, Mannheim, Germany.

In Vitro Culture of Immune Cell Populations

Myeloid cell populations were purified from the mesenteric lymph nodes of C57Bl/6 mice that had been orally infected with *T. gondii* cysts 5 days previously (see Extended Experimental Procedures). A total of 0.25×10^4–1.2×10^5 of the indicated myeloid cell populations was cultured with 0.5×10^5–2×10^5 NK cells overnight in 96-well round-bottom plates in RPMI supplemented with 10% FCS, L-glutamine, 2-ME, Pen/Strep, and 50 U/ml rhIL-2. For the final 4 hr of culture, GolgiStop and GolgiPlug (BD Biosciences) were added to cultures.

Statistics

Values are expressed as mean ± SEM. Levels of significance were calculated by the unpaired Student's t test using GraphPad Prism software. Differences were considered significant at $p < 0.05$ and are indicated with an asterisk. "ns" is not significant.

SUPPLEMENTAL INFORMATION

Supplemental Information includes Extended Experimental Procedures, two figures, and eight movies and can be found with this article online at http://dx.doi.org/10.1016/j.celrep.2012.06.001.

LICENSING INFORMATION

ACKNOWLEDGMENTS

REFERENCES

Andrews, D.M., Scalzo, A.A., Yokoyama, W.M., Smyth, M.J., and Degli-Esposti, M.A. (2003). Functional interactions between dendritic cells and NK cells during viral infection. Nat. Immunol. *4*, 175–181.

Arase, H., Saito, T., Phillips, J.H., and Lanier, L.L. (2001). Cutting edge: the mouse NK cell-associated antigen recognized by DX5 monoclonal antibody is CD49b (alpha 2 integrin, very late antigen-2). J. Immunol. *167*, 1141–1144.

Bajénoff, M., Breart, B., Huang, A.Y.C., Qi, H., Cazareth, J., Braud, V.M., Germain, R.N., and Glaichenhaus, N. (2006). Natural killer cell behavior in lymph nodes revealed by static and real-time imaging. J. Exp. Med. *203*, 619–631.

Baratin, M., Roetynck, S., Lépolard, C., Falk, C., Sawadogo, S., Uematsu, S., Akira, S., Ryffel, B., Tiraby, J.G., Alexopoulou, L., et al. (2005). Natural killer cell and macrophage cooperation in MyD88-dependent innate responses to *Plasmodium falciparum*. Proc. Natl. Acad. Sci. USA *102*, 14747–14752.

Barral, P., Polzella, P., Bruckbauer, A., van Rooijen, N., Besra, G.S., Cerundolo, V., and Batista, F.D. (2010). CD169+ macrophages present lipid antigens to mediate early activation of iNKT cells in lymph nodes. Nat. Immunol. *11*, 303–312.

Beuneu, H., Deguine, J., Breart, B., Mandelboim, O., Di Santo, J.P., and Bousso, P. (2009). Dynamic behavior of NK cells during activation in lymph nodes. Blood *114*, 3227–3234.

Biesen, R., Demir, C., Barkhudarova, F., Grün, J.R., Steinbrich-Zöllner, M., Backhaus, M., Häupl, T., Rudwaleit, M., Riemekasten, G., Radbruch, A., et al. (2008). Sialic acid-binding Ig-like lectin 1 expression in inflammatory and resident monocytes is a potential biomarker for monitoring disease activity and success of therapy in systemic lupus erythematosus. Arthritis Rheum. *58*, 1136–1145.

Borg, C., Jalil, A., Laderach, D., Maruyama, K., Wakasugi, H., Charrier, S., Ryffel, B., Cambi, A., Figdor, C., Vainchenker, W., et al. (2004). NK cell activation by dendritic cells (DCs) requires the formation of a synapse leading to IL-12 polarization in DCs. Blood *104*, 3267–3275.

Bousso, P., and Robey, E. (2003). Dynamics of CD8+ T cell priming by dendritic cells in intact lymph nodes. Nat. Immunol. *4*, 579–585.

Braun, A., Worbs, T., Moschovakis, G.L., Halle, S., Hoffmann, K., Bölter, J., Münk, A., and Förster, R. (2011). Afferent lymph-derived T cells and DCs use different chemokine receptor CCR7-dependent routes for entry into the lymph node and intranodal migration. Nat. Immunol. *12*, 879–887.

Brilot, F., Strowig, T., Roberts, S.M., Arrey, F., and Münz, C. (2007). NK cell survival mediated through the regulatory synapse with human DCs requires IL-15Ralpha. J. Clin. Invest. *117*, 3316–3329.

Carrasco, Y.R., and Batista, F.D. (2007). B cells acquire particulate antigen in a macrophage-rich area at the boundary between the follicle and the subcapsular sinus of the lymph node. Immunity *27*, 160–171.

Chtanova, T., Schaeffer, M., Han, S.J., van Dooren, G.G., Nollmann, M., Herzmark, P., Chan, S.W., Satija, H., Camfield, K., Aaron, H., et al. (2008). Dynamics of neutrophil migration in lymph nodes during infection. Infect. Immun. *29*, 487–496.

Chtanova, T., Han, S.J., Schaeffer, M., van Dooren, G.G., Herzmark, P., Striepen, B., and Robey, E.A. (2009). Dynamics of T cell, antigen-presenting cell, and pathogen interactions during recall responses in the lymph node. Immunity *31*, 342–355.

Coombes, J.L., and Robey, E.A. (2010). Dynamic imaging of host-pathogen interactions in vivo. Nat. Rev. Immunol. *10*, 353–364.

Combe, C.L., Curiel, T.J., Moretto, M.M., and Khan, I.A. (2005). NK cells help to induce CD8(+)-T-cell immunity against *Toxoplasma gondii* in the absence of CD4(+) T cells. Infect. Immun. *73*, 4913–4921.

Dalbeth, N., Gundle, R., Davies, R.J., Lee, Y.C., McMichael, A.J., and Callan, M.F. (2004). CD56bright NK cells are enriched at inflammatory sites and can engage with monocytes in a reciprocal program of activation. J. Immunol. *173*, 6418–6426.

Denkers, E.Y., Gazzinelli, R.T., Martin, D., and Sher, A. (1993). Emergence of NK1.1+ cells as effectors of IFN-gamma dependent immunity to *Toxoplasma gondii* in MHC class I-deficient mice. J. Exp. Med. *178*, 1465–1472.

Dunay, I.R., Damatta, R.A., Fux, B., Presti, R., Greco, S., Colonna, M., and Sibley, L.D. (2008). Gr1(+) inflammatory monocytes are required for mucosal resistance to the pathogen *Toxoplasma gondii*. Immunity *29*, 306–317.

Ferlazzo, G., Pack, M., Thomas, D., Paludan, C., Schmid, D., Strowig, T., Bougras, G., Muller, W.A., Moretta, L., and Münz, C. (2004). Distinct roles of IL-12 and IL-15 in human natural killer cell activation by dendritic cells from secondary lymphoid organs. Proc. Natl. Acad. Sci. USA *101*, 16606–16611.

Fernandez, N.C., Lozier, A., Flament, C., Ricciardi-Castagnoli, P., Bellet, D., Suter, M., Perricaudet, M., Tursz, T., Maraskovsky, E., and Zitvogel, L. (1999). Dendritic cells directly trigger NK cell functions: cross-talk relevant in innate anti-tumor immune responses in vivo. Nat. Med. *5*, 405–411.

Garrod, K.R., Wei, S.H., Parker, I., and Cahalan, M.D. (2007). Natural killer cells actively patrol peripheral lymph nodes forming stable conjugates to eliminate MHC-mismatched targets. Proc. Natl. Acad. Sci. USA *104*, 12081–12086.

Gazit, R., Gruda, R., Elboim, M., Arnon, T.I., Katz, G., Achdout, H., Hanna, J., Qimron, U., Landau, G., Greenbaum, E., et al. (2006). Lethal influenza infection in the absence of the natural killer cell receptor gene Ncr1. Nat. Immunol. *7*, 517–523.

Gazzinelli, R.T., Hieny, S., Wynn, T.A., Wolf, S., and Sher, A. (1993). Interleukin 12 is required for the T-lymphocyte-independent induction of interferon gamma by an intracellular parasite and induces resistance in T-cell-deficient hosts. Proc. Natl. Acad. Sci. USA *90*, 6115–6119.

Gazzinelli, R.T., Wysocka, M., Hayashi, S., Denkers, E.Y., Hieny, S., Caspar, P., Trinchieri, G., and Sher, A. (1994). Parasite-induced IL-12 stimulates early IFN-gamma synthesis and resistance during acute infection with *Toxoplasma gondii*. J. Immunol. *153*, 2533–2543.

Goldszmid, R.S., Bafica, A., Jankovic, D., Feng, C.G., Caspar, P., Winkler-Pickett, R., Trinchieri, G., and Sher, A. (2007). TAP-1 indirectly regulates CD4+ T cell priming in *Toxoplasma gondii* infection by controlling NK cell IFN-gamma production. J. Exp. Med. *204*, 2591–2602.

Gray, E.E., Friend, S., Suzuki, K., Phan, T.G., and Cyster, J.G. (2012). Subcapsular sinus macrophage fragmentation and CD169(+) Bleb acquisition by closely associated IL-17-committed innate-like lymphocytes. PLoS One *7*, e38258.

Guan, H., Moretto, M., Bzik, D.J., Gigley, J., and Khan, I.A. (2007). NK cells enhance dendritic cell response against parasite antigens via NKG2D pathway. J. Immunol. *179*, 590–596.

Hou, B., Benson, A., Kuzmich, L., DeFranco, A.L., and Yarovinsky, F. (2011). Critical coordination of innate immune defense against *Toxoplasma gondii* by dendritic cells responding via their Toll-like receptors. Proc. Natl. Acad. Sci. USA *108*, 278–283.

Hunter, C.A., Subauste, C.S., Van Cleave, V.H., and Remington, J.S. (1994). Production of gamma interferon by natural killer cells from *Toxoplasma gondii*-infected SCID mice: regulation by interleukin-10, interleukin-12, and tumor necrosis factor alpha. Infect. Immun. *62*, 2818–2824.

Iannacone, M., Moseman, E.A., Tonti, E., Bosurgi, L., Junt, T., Henrickson, S.E., Whelan, S.P., Guidotti, L.G., and von Andrian, U.H. (2010). Subcapsular sinus macrophages prevent CNS invasion on peripheral infection with a neurotropic virus. Nature *465*, 1079–1083.

Ivanov, I.I., Frutos, Rde.L., Manel, N., Yoshinaga, K., Rifkin, D.B., Sartor, R.B., Finlay, B.B., and Littman, D.R. (2008). Specific microbiota direct the differentiation of IL-17-producing T-helper cells in the mucosa of the small intestine. Cell Host Microbe *4*, 337–349.

Ivanov, I.I., Atarashi, K., Manel, N., Brodie, E.L., Shima, T., Karaoz, U., Wei, D., Goldfarb, K.C., Santee, C.A., Lynch, S.V., et al. (2009). Induction of intestinal Th17 cells by segmented filamentous bacteria. Cell *139*, 485–498.

Johnson, L.L., VanderVegt, F.P., and Havell, E.A. (1993). Gamma interferon-dependent temporary resistance to acute *Toxoplasma gondii* infection independent of CD4+ or CD8+ lymphocytes. Infect. Immun. *61*, 5174–5180.

Junt, T., Moseman, E.A., Iannacone, M., Massberg, S., Lang, P.A., Boes, M., Fink, K., Henrickson, S.E., Shayakhmetov, D.M., Di Paolo, N.C., et al. (2007). Subcapsular sinus macrophages in lymph nodes clear lymph-borne viruses and present them to antiviral B cells. Nature *450*, 110–114.

Kang, S.J., Liang, H.E., Reizis, B., and Locksley, R.M. (2008). Regulation of hierarchical clustering and activation of innate immune cells by dendritic cells. Immunity *29*, 819–833.

Kassim, S.H., Rajasagi, N.K., Zhao, X., Chervenak, R., and Jennings, S.R. (2006). In vivo ablation of CD11c-positive dendritic cells increases suscepti-bility to herpes simplex virus type 1 infection and diminishes NK and T-cell responses. J. Virol. *80*, 3985–3993.

Khan, I.A., Matsuura, T., and Kasper, L.H. (1994). Interleukin-12 enhances murine survival against acute toxoplasmosis. Infect. Immun. *62*, 1639–1642.

Khan, I.A., Thomas, S.Y., Moretto, M.M., Lee, F.S., Islam, S.A., Combe, C., Schwartzman, J.D., and Luster, A.D. (2006). CCR5 is essential for NK cell traf-ficking and host survival following *Toxoplasma gondii* infection. PLoS Pathog. *2*, e49.

Klezovich-Bénard, M., Corre, J.P., Jusforgues-Saklani, H., Fiole, D., Burjek, N., Tournier, J.N., and Goossens, P.L. (2012). Mechanisms of NK cell-macro-phage *Bacillus anthracis* crosstalk: a balance between stimulation by spores and differential disruption by toxins. PLoS Pathog. *8*, e1002481.

Koka, R., Burkett, P., Chien, M., Chai, S., Boone, D.L., and Ma, A. (2004). Cutting edge: murine dendritic cells require IL-15R alpha to prime NK cells. J. Immunol. *173*, 3594–3598.

Lucas, M., Schachterle, W., Oberle, K., Aichele, P., and Diefenbach, A. (2007). Dendritic cells prime natural killer cells by trans-presenting interleukin 15. Immunity *26*, 503–517.

Martín-Fontecha, A., Thomsen, L.L., Brett, S., Gerard, C., Lipp, M., Lanzavec-chia, A., and Sallusto, F. (2004). Induced recruitment of NK cells to lymph nodes provides IFN-gamma for T(H)1 priming. Nat. Immunol. *5*, 1260–1265.

Mashayekhi, M., Sandau, M.M., Dunay, I.R., Frickel, E.M., Khan, A., Gold-szmid, R.S., Sher, A., Ploegh, H.L., Murphy, T.L., Sibley, L.D., and Murphy, K.M. (2011). CD8α(+) dendritic cells are the critical source of interleukin-12 that controls acute infection by *Toxoplasma gondii* tachyzoites. Immunity *35*, 249–259.

Miyake, S., Sakurai, T., Okumura, K., and Yagita, H. (1994). Identification of collagen and laminin receptor integrins on murine T lymphocytes. Eur. J. Immunol. *24*, 2000–2005.

Mortier, E., Woo, T., Advincula, R., Gozalo, S., and Ma, A. (2008). IL-15Ralpha chaperones IL-15 to stable dendritic cell membrane complexes that activate NK cells via trans presentation. J. Exp. Med. *205*, 1213–1225.

Newman, K.C., and Riley, E.M. (2007). Whatever turns you on: accessory-cell-dependent activation of NK cells by pathogens. Nat. Rev. Immunol. *7*, 279–291.

Phan, T.G., Grigorova, I., Okada, T., and Cyster, J.G. (2007). Subcapsular encounter and complement-dependent transport of immune complexes by lymph node B cells. Nat. Immunol. *8*, 992–1000.

Phan, T.G., Green, J.A., Gray, E.E., Xu, Y., and Cyster, J.G. (2009). Immune complex relay by subcapsular sinus macrophages and noncognate B cells drives antibody affinity maturation. Nat. Immunol. *10*, 786–793.

Pribul, P.K., Harker, J., Wang, B., Wang, H., Tregoning, J.S., Schwarze, J., and Openshaw, P.J. (2008). Alveolar macrophages are a major determinant of early responses to viral lung infection but do not influence subsequent disease development. J. Virol. *82*, 4441–4448.

Roozendaal, R., Mebius, R.E., and Kraal, G. (2008). The conduit system of the lymph node. Int. Immunol. *20*, 1483–1487.

Schaeffer, M., Han, S.J., Chtanova, T., van Dooren, G.G., Herzmark, P., Chen, Y., Roysam, B., Striepen, B., and Robey, E.A. (2009). Dynamic imaging of T cell-parasite interactions in the brains of mice chronically infected with *Toxoplasma gondii*. J. Immunol. *182*, 6379–6393.

Schleicher, U., Liese, J., Knippertz, I., Kurzmann, C., Hesse, A., Heit, A., Fischer, J.A., Weiss, S., Kalinke, U., Kunz, S., and Bogdan, C. (2007). NK cell activation in visceral leishmaniasis requires TLR9, myeloid DCs, and IL-12, but is independent of plasmacytoid DCs. J. Exp. Med. *204*, 893–906.

Soderquest, K., Powell, N., Luci, C., van Rooijen, N., Hidalgo, A., Geissmann, F., Walzer, T., Lord, G.M., and Martín-Fontecha, A. (2011). Monocytes control natural killer cell differentiation to effector phenotypes. Blood *117*, 4511–4518.

Van Rooijen, N., and Sanders, A. (1994). Liposome mediated depletion of macrophages: mechanism of action, preparation of liposomes and applica-tions. J. Immunol. Methods *174*, 83–93.

Walzer, T., Bléry, M., Chaix, J., Fuseri, N., Chasson, L., Robbins, S.H., Jaeger, S., André, P., Gauthier, L., Daniel, L., et al. (2007). Identification, activation, and selective in vivo ablation of mouse NK cells via NKp46. Proc. Natl. Acad. Sci. USA *104*, 3384–3389.

White, D.J., Puranen, S., Johnson, M.S., and Heino, J. (2004). The collagen receptor subfamily of the integrins. Int. J. Biochem. Cell Biol. *36*, 1405–1410.